JOURNAL OF CATALYSIS 145, 276–288 (1994)

Effect of Thermal Treatments on the Properties of Nickel and Cobalt Activated-Charcoal-Supported Catalysts

L. M. Gandia and M. Montes

Grupo de Ingeniería, Departamento de Química Aplicada, Facultad de Química de San Sebastian, Universidad del País Vasco, Apdo. 1072, 20080 San Sebastián, Spain

Received January 5, 1993; revised July 28, 1993

The effect of thermal pretreatment in N_2 up to 723 K and the activation treatments in H_2 and an inert atmosphere on the properties of Ni and Co activated-charcoal-supported catalysts were studied. Catalysts were characterized by means of N_2 adsorption at 77 K, H_2 chemisorption at room temperature, thermogravimetric analysis (TGA), X-ray diffraction (XRD), and transmission electron microscopy (TEM). The catalysts' activity and selectivity for acetone hydrogenation to 2-propanol under unusual and severe conditions (473 K and high overall acetone conversion) were also measured. TGA and XRD evidence was found for the charcoal-support-promoted NiO and CoO reduction to the metallic states when the catalysts were subjected to an inert atmosphere at 723 K. The thermal activation treatments under H_2 or inert atmosphere above 723 K caused a loss of acetone hydrogenation activity (calculated on a metal load basis) for both the Ni and Co activated-charcoal-supported catalysts, with respect to that of the low-temperature (573 K) activation treatments. In a series of activated-charcoal-supported Ni catalysts, a large decrease in the H_2 chemisorption uptake was also found for a sample pretreated in N_2 at 723 K prior to H_2 reduction. These results were not due to nickel or cobalt sintering, as shown by XRD line broadening measurements. The catalytic activity loss was accompanied by a decrease (in the case of Ni) and an increase (in the case of Co) in the 2-propanol selectivity.

INTRODUCTION

The use of carbon in catalysis is continuously increasing. Its application as a catalyst support offers several advantages (1, 2). Carbon is cheap and is a relatively inert material. After an activation process, a porous network is developed which gives very high surface areas. Furthermore, expensive supported precious metals can be easily recovered by burning off the carbonaceous support. Recently, the use of carbon as a support in sulfide catalysts for HDS and HDN processes has been claimed (3, 4). In such way Ni and Co sulfides have hydrodesulfurizing activities which are comparable and higher, respectively, than those of the typical γ-alumina-supported catalysts. Oyama *et al.* (5, 6) have studied a new, very interesting application of carbon, not as support, but as an intrinsic catalytic component in the form of transition metal carbides. These authors reported activities for several carbides (e.g., Mo_2C, WC, ...) which resemble or even exceed those of the platinum group metals in a wide variety of reactions.

In this work, attention has been focused on the effect of thermal treatments on the properties of nickel and cobalt activated-charcoal supported catalysts. High-temperature treatments are of great importance in this case since very intense interactions can be promoted in metal/carbon systems. These interactions play a major role conditioning both textural properties and reactivity of the catalyst. These aspects are briefly summarized. The dispersion of a supported metal is one of the main parameters related to its catalytic activity. When carbon is the support, metallic dispersion can be more or less controlled by means of the thermal and chemical modification of the support porous structure and surface oxygenated complexes (7–10). In addition, these surface oxygenated functional groups control the acidic character of the catalyst (2, 11). The acidic strength can vary over a wide range as a function of the elaboration method and the raw material source employed to obtain the carbon support (1). The nature of the metallic phase present in the catalyst can also be influenced by the reducing properties of the carbon. In this way, carbon is able to reduce the metal precursor introduced during the catalyst preparation. This is the case for the reduction of palladium nitrate to Pd metal (1), MoO_3 to MoO_2 and Mo (12), NiO to Ni (13), and CoO to Co (13, 14).

On the other hand, the well known activity of the transition metals for the gasification of carbon (15) is due to the interactions established between these metals and the carbonaceous materials. The mechanism of such interactions is mainly dependent on the temperature, the metal, the kind of carbon employed as well as the nature of the gaseous atmosphere. The graphite gasification reaction has been widely studied. Under an oxidizing atmosphere, phenomena such as dissolution and diffusion of carbon atoms into the metal (16) and metal particles undergoing

0021-9517/94 $5.00

redox cycles between the oxide and metallic states accounting for the oxygen transfer to the graphite (14, 17) are involved. Under a reducing atmosphere the catalytic particle is in the metallic state. The hydrogenation of graphite starts at about 1100 K with the metal particle cutting well defined channels across the graphitic structure (14, 16, 18, 19). Temperatures at which metal–carbon interactions occur do not necessarily have to be too high. Thus, for a 600-K surface-carburized Ni polycrystalline foil, the diffusion of carbon atoms into the bulk has been reported above this temperature (20).

In addition to site blocking, the presence of surface carbon during chemisorption on transition metals can produce other phenomena such as higher activation energy barriers and lower binding energies for H_2 chemisorption (21), or a redistribution towards lower binding energy states for CO chemisorption (20).

Carbons used as catalytic support are normally associated with relatively high amounts of inorganic compounds that can alter the catalytic behaviour. After the activation process, the carbon surface is enriched with these impurities that can catalyze nondesired reactions, alter the sintering resistence of the supported metals, or act as catalysts poisons (8, 22). The nature of the inorganic residue is highly dependent on the raw material source, with sulfur, iron, silica, and alkali and alkaline earth metals being the most common. Albers *et al.* found that the activity of a platinum on activated carbon catalyst for the cinnamic acid hydrogenation linearly decreased with increasing amounts of surface Ca or Fe (2). Sulfur can be present in carbon as the free element, combined with metals, and as organic sulfur. It seems that all is chemically bonded with the carbon (11). Sulfur poisoning of transition metals via formation of very stable surface sulfides is well known (23), hence metals supported on sulfur-containing carbons can be poisoned to different extents, depending on the thermal treatments they have undergone.

Taking into account the variety of phenomena and experimental conditions under which they occur, it is clear that the temperatures involved in the preparation and characterization of charcoal-supported catalysts must be carefully selected to avoid any undesirable effect related to the metal/carbon interactions.

The aim of this work was to study nickel and cobalt activated-charcoal-supported catalysts. The effect of thermal treatment under N_2 up to 723 K and the reduction temperature under H_2 at 573 or 773 K were considered. The treated samples were characterized by means of N_2 adsorption, thermogravimetric analysis (TGA), X-ray diffraction (XRD), transmission electron microscopy (TEM) for one sample to check XRD line broadening data, and H_2 chemisorption (for Ni samples). The catalytic activity and selectivity for a wide range of overall acetone conversions of the resulting catalysts for the high-temperature (473 K) acetone hydrogenation were measured. The catalytic behaviour of unsupported Ni and Co powders as well as that of partially sulfurized Ni and Co on activated-charcoal catalysts was also studied. The nonconventional reaction conditions (high temperature and conversion) chosen for this study are related to the possibility of using the catalytic system acetone/H_2/2-propanol in a high-temperature chemical heat pump for waste heat recovery (24).

TABLE 1

Activation Treatment Procedures Employed in This Work

Abbreviation	Activation treatment procedure
A	H_2 reduction for 12 h at 573 K
B	H_2 reduction for 12 h at 573 K, followed by purge in inert gas for 20 min at 773 K
C	Inert gas flow treatment for 12 h at 723 K
D	H_2 reduction for 12 h at 773 K
E	H_2 reduction for 12 h at 573 K, followed by purge in inert gas for 3 h at 773 K

EXPERIMENTAL

Catalysts

Two parent catalysts were prepared by the incipient wetness technique. In this way, the required amount of an aqueous solution of $Ni(NO_3)_2 \cdot 6H_2O$ or $Co(NO_3)_2 \cdot 6H_2O$ (Merck, analytical reagent grade) was slowly added to the support (100–200 μm size fraction) to obtain catalysts with ca. 10 wt% metallic content. The support used was a commercial (Norit ROX 0.8) acid-washed activated carbon with ash content up to 3 wt%, S content up to 0.7 wt%, and Fe and Ca contents lower than 0.02 wt%. After impregnation the samples were dried overnight at 343 K and they are referred to as (C–Ni) and (C–Co), respectively. Three additional samples were prepared from (C–Ni) and two from (C–Co) by treatment for 12 h at 423 (only with Ni), 573, and 773 K in a stream of 80 ml min^{-1} g^{-1} of N_2 (SEO 99.9995%, treated with a Chrompack clean oxygen filter). These new samples are referred to as (C–Ni) or (C–Co) followed by the respective N_2 pretreatment temperature (K), e.g., (C–Ni)423, (C–Co)723, etc. The effect of thermal pretreatment in N_2 on the support (C) has also been considered and three new samples were obtained and referred to as (C) followed by the pretreatment temperature, e.g., (C)423, (C)573, etc.

In order to study the influence of the reduction conditions on the catalyst properties, several different activation treatments were used. These activation treatments referred to as A to E are described in Table 1.

Ni and Co powders were prepared carefully, by passivating at ambient temperature with an Ar stream containing

100 ppm O_2 the solids that resulted from a 12-h H_2 reduction of NiO and Co_3O_4 powders at 773 K. These oxides were obtained from air decomposition of the respective nitrates (Merck). To obtain partially sulfurized catalysts the (C–Ni) and (C–Co) samples were subjected to activation treatment A, and subsequent benzene hydrogenation at 473 K with 100 ppm H_2S in the feed (10 mol% benzene in H_2). The extent of poisoning was controlled by means of the benzene to cyclohexane conversion, the reaction being stopped when the conversion had decreased to 10% of its initial value.

In order to measure the metallic content, catalysts (50 mg) were extracted by aqua regia (4 ml) plus HF (6 ml) in an ultrasonic bath for 1.5 h at 353 K. Ni contents were obtained by the EDTA/murexide titration of the resulting filtered solutions. Co content was spectrophotometrically determined by the thiocyanate method (25).

Nitrogen Adsorption

The N_2 adsorption/desorption isotherms at 77 K of the samples were obtained in a Micromeritics ASAP 2000. Samples were previously degassed for 2h at 473 K and 10^{-3} Torr (1 Torr = 133.3 N m^{-2}). The BET equation was used to calculate the specific surface area. The external specific surface area (outside the micropores) was obtained from the respective *t*-plots. The micropore surface area was evaluated as the difference between the BET and the external surface areas.

Thermogravimetric Analysis (TGA)

Thermogravimetric experiments were carried out in a Setaram TG 85 thermobalance. Two series of experiments were made with either a flow of N_2 (SEO 99.9995%) or H_2 (SEO 99.999%), both gases being further purified with oxygen and hydrocarbon filters (Chrompack). Samples (28 mg) were loaded into the thermobalance and heated under 20 ml min^{-1} of the desired gas at 423 K until constant weight was achieved. Then, the weight loss rate was recorded between 423 and 1273 K with a controlled heating rate of 8 K min^{-1}.

X-Ray Diffraction (XRD)

XRD patterns were obtained with a Philips APD 1710 powder diffractometer. Nickel filtered Cu K_α radiation was employed covering 2θ angles between 10° and 85°. The mean crystallite diameters were estimated from application of the Scherrer equation. The width of the Ni (111) and Co (111) peaks at half-maximum was corrected for K_α doublet and instrumental broadening (26).

Transmission Electron Microscopy (TEM)

In order to check XRD line broadening data, electron microscopy observations of the (C–Ni)723 catalyst were carried out in a Hitachi 7000FA microscope. The sample was previously reduced for 12 h at 573 K in flowing H_2, then cooled to room temperature, and passivated for 1 h with an Ar stream containing 100 ppm O_2. Samples were ground in an agate mortar and then ultrasonically dispersed in isopropyl alcohol. Some drops of the resulting dispersion were deposited on a standard copper grid previously covered with a carbon film.

Metallic Surface Area

The Ni surface area (S_{Ni}) was measured by H_2 chemisorption with a Micromeritics Pulse Chemisorb 2700. Catalysts were previously reduced for 12 h at 573 K with 80 ml min^{-1} of H_2 (SEO 99.999%). After reduction the hydrogen on the nickel surface was removed with 15 ml min^{-1} of N_2 (SEO 99.999%, treated with a Chrompack clean-oxygen filter) for 20 min at 773 K. The sample was subsequently cooled to room temperature under the same N_2 stream and H_2 pulses (0.047 ml) were injected until the eluted area of consecutive pulses was constant. Nickel surface areas were calculated assuming a stoichiometry of 1 hydrogen molecule adsorbed per 2 surface nickel atoms, and an area of 6.33 $Å^2$ by each exposed nickel atom (27). The available flow technique was not satisfactory for the cobalt surface area measurement due to the highly reversible character of the hydrogen chemisorption over cobalt (21, 28).

Acetone Hydrogenation

Acetone hydrogenation reactions were carried out in a fixed-bed reactor at 473 K and atmospheric pressure. The acetone (Panreac P.A.) was previously treated with P_2O_5 under reflux for 5 h, then distilled over activated molecular sieve and finally stored in two thermostated (283 K) gas saturators. The saturators were kept at 1.5 atm (1 atm = 101.3×10^3 N m^{-2}) absolute pressure by means of a Brooks 5866 pressure controller in order to set constant the feed stream composition at 10 mol% acetone and 90 mol% hydrogen. The H_2 flow rate coming into the saturators was controlled by a Brooks 5850 TR mass flow controller. The reaction products were analysed by online gas chromatography (Hewlett–Packard 5710A). Prior to reaction, catalysts were subjected to different in situ activation treatments, which are summarized in Table 1. Experiments were carried out at different W/F_{A0} values to evaluate the overall acetone conversion and selectivity for the different reaction products. Reaction rates were measured in differential reactor conditions and referred to the total amount of metal loaded in the reactor. Selectiv-

TABLE 2

Metallic Content, BET Surface Area (S_{BET}), Microporous Surface Area (S_m), and External Surface Area (S_e) of the Thermally Pretreated Samples

Sample	Metallic content (wt%)	S_{BET} ($m^2\ g_{cat}^{-1}$)	S_m ($m^2\ g_{cat}^{-1}$)	S_e ($m^2\ g_{cat}^{-1}$)
C		1265	1183	82
C423		1213	1126	87
C573		1298	1210	88
C773		1265	1187	77
(C–Ni)	9.77	516	468	48
(C–Ni)423	9.99	530	488	42
(C–Ni)573	11.22	815	768	47
(C–Ni)773	11.13	923	862	61
(C–Co)	11.50	681	630	51
(C–Co)573	[a]	795	735	60
(C–Co)773	[a]	992	922	70

[a] Not measured.

ities were defined as the molar fraction of the reacted acetone which was converted into a given product.

RESULTS

Nitrogen Adsorption

Table 2 presents the BET specific surface area (S_{BET}), micropore surface area (S_m), external surface area (S_e), and the metallic content (wt%) of the prepared samples. It can be seen that the textural parameters of the support remained constant after N_2 pretreatments at different temperatures up to 723 K. The impregnation process with Ni or Co nitrate solutions produced a dramatic decrease in both S_m and S_e that was not restored by drying. When the parent catalysts were treated under flowing N_2 at progressively higher temperature, a specific surface area partial recovery took place.

Thermogravimetric Analysis (TGA)

Figure 1 shows the weight loss rate obtained under N_2 for the support (C) (Fig. 1a) and (C–Ni) (Fig. 1b), (C–Ni)723 (Fig. 1c), and (C–Co) (Fig. 1d) samples at constant heating rate. The support showed a total weight loss of 3.5% with a maximum at 573 K. The (C–Ni) catalyst showed a broad low-temperature peak in the range between 423 and 623 K, and a sharp high-temperature peak at 800 K. At higher temperatures the weight loss was slow and continuous. The (C–Ni)723 catalyst only showed a small sharp peak at 821 K. The (C–Co) catalyst showed a broad low-temperature peak between 423 and 523 K, and a sharp high-temperature peak at 825 K.

Figure 2 shows the weight loss rate obtained in a stream of H_2 for the support (C) (Fig. 2a) and (C–Ni) (Fig. 2b), (C–Ni)723 (Fig. 2c), and (C–Co) (Fig. 2d) samples. The

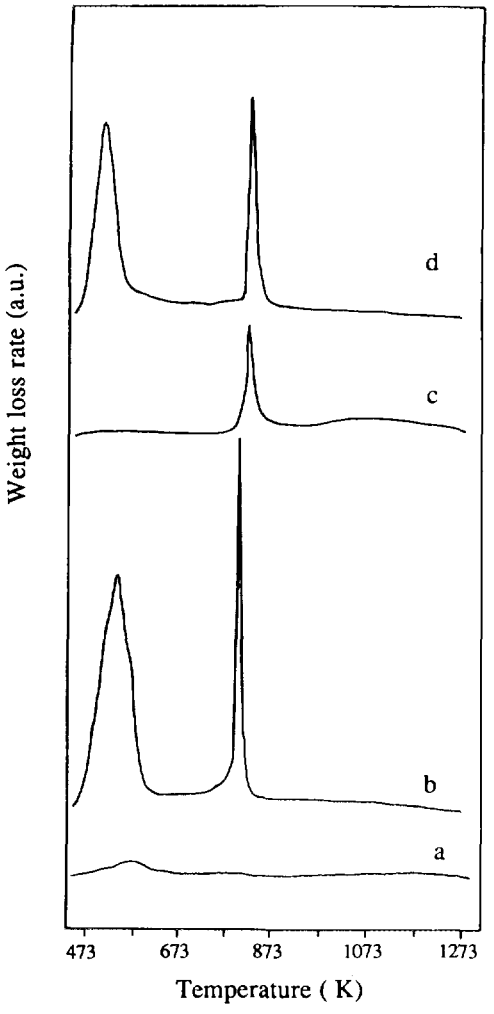

FIG. 1. Weight loss rate profiles in N_2 of the samples (C) (a), (C–Ni) (b), (C–Ni)723 (c), and (C–Co) (d).

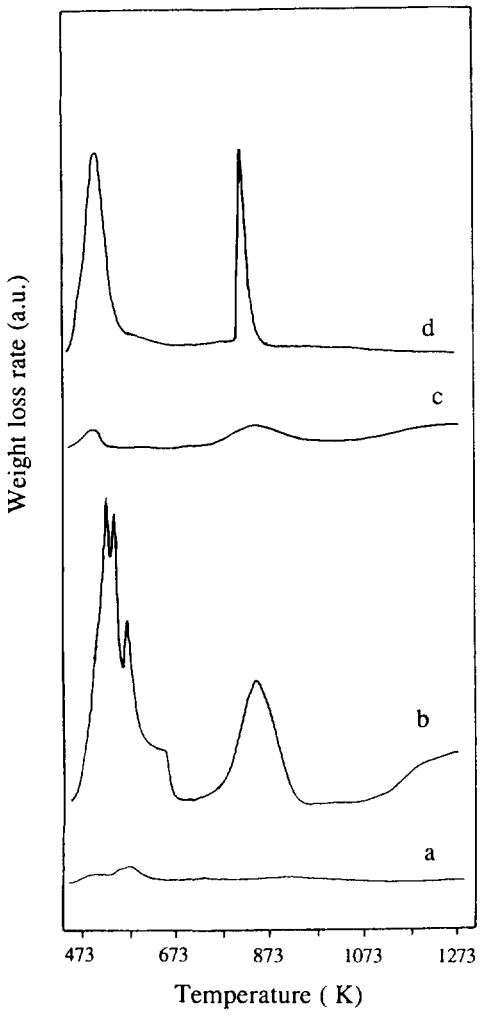

FIG. 2. Weight loss rate profiles in H_2 of the samples (C) (a), (C–Ni) (b), (C–Ni)723 (c), and (C–Co) (d).

support and (C–Co) catalyst behaved in a similar way as they did in N_2. However, the (C–Ni) catalyst low-temperature peak was resolved into three well defined peaks in the same temperature range. The second peak became broader corresponding to a greater weight loss and was displaced to 845 K. The (C–Ni)723 catalyst high-temperature peak was also broader in H_2 than in N_2 and displaced to 857 K. The two Ni-containing catalysts showed an increasing weight loss rate above 1100 K when treated in H_2.

X-Ray Diffraction (XRD)

Figures 3 and 4 show the XRD patterns of the support (Fig. 3) and (C–Ni) (Fig. 4) samples pretreated in flowing N_2 at different temperatures, cooled to room temperature, and then exposed to air. XRD patterns of the support correspond to an amorphous material and do not show

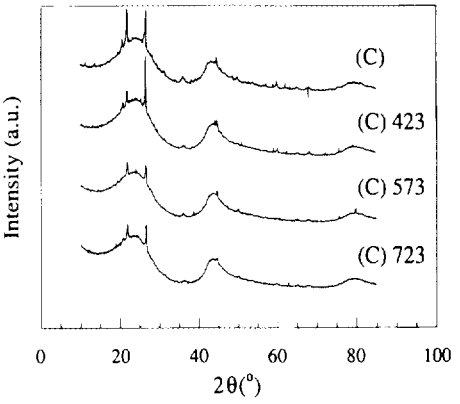

FIG. 3. XRD patterns of the activated charcoal support (C) subjected to N_2 thermal pretreatments at 423, 573, and 723 K.

significant modification by N_2 thermal pretreatment up to 723 K (Fig. 3). Two sharp peaks can be observed in this figure. The first at 22° is due to the presence of silica (cristobalite); the second at 26.6° can be assigned to crystalline graphitic carbon. The (C–Ni) catalyst XRD pattern is very similar to that of the support, but pretreatments in N_2 at increasing temperatures progressively showed peaks corresponding to nickel oxide at 573 K and metallic nickel at 723 K (Fig. 4).

Figure 5 shows the XRD patterns of the (C–Co), (C–Co)573, and (C–Co)723 samples. There is no difference between support and (C–Co) sample XRD patterns. The (C–Co)573 sample shows broad diffraction peaks at 36.8°, 42.8°, and 61.8° corresponding to CoO. The phase identification in the (C–Co)723 XRD pattern is very difficult to determine due to the broadening and the proximity of the diffraction peaks for different cobalt phases. A broad peak at 36.7° is shown which probably corresponds to Co_3O_4. The (fcc) Co metallic phase is also likely to be present, as it can be deduced from the peak at 44.3°.

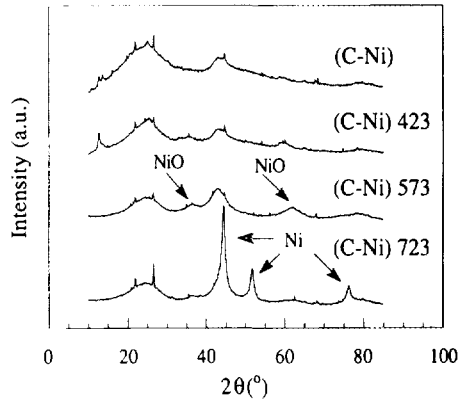

FIG. 4. XRD patterns of the (C–Ni) sample subjected to N_2 thermal pretreatments at 423, 573, and 723 K.

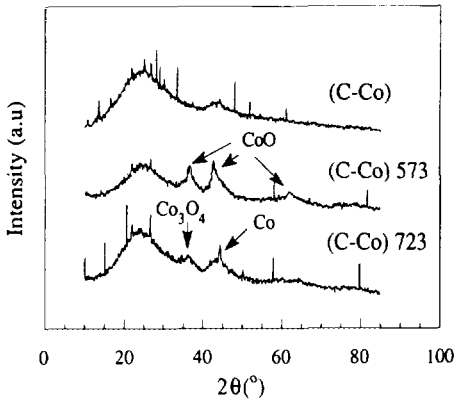

FIG. 5. XRD patterns of the (C–Co) sample subjected to N_2 thermal pretreatments at 573 and 723 K.

Conventional X-ray diffraction line broadening (XRDLB) calculations have been performed in order to estimate the metallic crystallite diameter. These results are summarized in Table 3. Samples were subjected to the same activation treatments that were employed in metallic surface area and catalytic activity measurements. After these treatments, samples were cooled to room temperature and carefully passivated with a stream of Ar containing 100 ppm O_2. XRD patterns have been obtained for the reduced and passivated samples; therefore, the diameters reported in Table 3 should be corrected to compensate for the passivation layers. Previous results (29) showed that the passivation treatment could oxidize 2 to 7 monolayers, suggesting that the crystallite size reported in Table 3 should be increased by 1 to 3 nm. Nevertheless, this lack of precision does not affect the analysis of the results, based on the comparison between sample activation treatments. The cobalt activated-charcoal-supported catalysts are probably more affected by the passivating oxide layers since cobalt is about 25 times easier to oxidize than nickel at room temperature (30). The cobalt catalysts which have been submitted to activation treatments above 573 K (flowing inert gas purge or flowing H_2 reduction at 773 K) show XRD patterns with very broad peaks of Co_3O_4 and metallic Co phases after room temperature passivation. This leads to a picture with the smallest particles probably being fully oxidized to Co_3O_4 and the remainder being covered by an oxide layer of noticeable thickness.

TABLE 3

Mean Crystallite Diameter (d_{XRD}), Nickel Surface Area (S_{Ni}), and Acetone Consumption Rate ($-r_A$) of the (C–Ni) and (C–Co) Samples after Different Activation Treatments[a]

Sample	d_{XRD} (nm)[b]	S_{Ni}(m^2 g_{Ni}^{-1})	$(-r_A)$ ($mol_{acetone}$ h^{-1} g_{metal}^{-1})[c]
(C–Ni)	A 12.5		A 7.5
(C–Ni)	B 12.2	B 5.0	B 1.6
(C–Ni)423	A 13.2	B 4.9	A 9.6
(C–Ni)573	A 11.9	B 4.6	A 10.5
(C–Ni)723	A 11.9	B 1.1	A 1.4
(C–Ni)	C 10.0		C 0.4
(C–Ni)	D 16.1		D 0.1
(C–Ni)723	D 16.1		
(C–Co)	A 15.3		A 14.5
(C–Co)	B 12.7		B 12.3
(C–Co)			E 7.4
(C–Co)	C 17.3		C 7.0
(C–Co)	D 9.1		D 1.0

[a] Each figure in this table is preceded by the respective abbreviation of the activation treatment that has been used (see Table 1).

[b] Measured by XRD line broadening.

[c] Acetone hydrogenation was carried out at 1 atm and 473 K with a feed stream containing 10 mol% acetone in H_2.

As can be seen from Table 3 the metallic crystallite size of the (C–Ni) catalyst does not show dramatic changes with the different treatments used. When the (C–Ni) catalyst is treated in flowing inert gas for 12 h at 773 K, the Ni metallic phase is developed (Fig. 4) and a crystallite size similar to that obtained after H_2 reduction at 573 K is obtained. If the (C–Ni) catalyst reduction temperature is increased from 573 to 773 K, the Ni particle diameter increases from 12.5 to 16.1 nm, showing a little sintering.

As was stated above, the cobalt particle diameters would be seriously affected by the passivating oxide layers. With the (C–Co) catalyst, the cobalt particles seem to diminish in size with increasing activation treatment temperature. In this way, 15.3-nm particles are obtained after H_2 stream reduction at 573 K. This value decreases to 12.7 nm with an Ar stream purge for 20 min at 773 K after reduction at 573 K, and to 9.1 nm after H_2 reduction for 12 h at 773 K. However, a higher value of 17.3 nm is obtained after Ar treatment for 12 h at 723 K.

TEM

Figure 6 shows the nickel particle diameter distribution obtained with the (C–Ni)723 catalyst after reduction in H_2 12 h at 573 K and passivation at room temperature, on the basis of 1100 counted particles. The particle size includes the passivation oxide layer. A more detailed observation of particles larger than 25 nm showed that they were formed by aggregation of smaller ones. Thus, no averaged values were calculated. Nevertheless, Fig. 6 shows an excellent agreement with the crystallite size obtained by XRDLB for this sample (12.5 nm).

Hydrogen Chemisorption

Metallic surface areas of the different (C–Ni) catalysts are reported in Table 3. A remarkable decrease in the nickel surface area can be seen for the (C–Ni)723 sample.

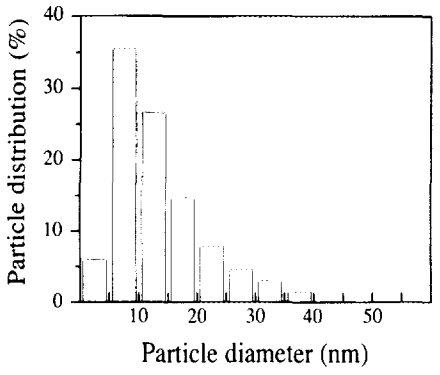

FIG. 6. Particle size distribution of the H_2 reduced at 573 K and room temperature passivated (C–Ni)723 sample.

When the (C–Ni) sample was treated in a N_2 stream for 12 h at 723 K and then cooled to room temperature, very little H_2 chemisorption takes place, hence no accurate measurement could be performed. This was also the case of the (C–Ni) catalyst when the reduction step was performed in H_2 at 773 K.

Catalytic Activity

(i) Acetone hydrogenation reaction rate. In this work, acetone hydrogenation rates have been reported on a metal load basis for comparison purposes, since cobalt metallic areas were not available. Furthermore, the reported metallic Ni surface areas are likely to be affected by the required cleaning purge in N_2 at 773 K prior to room temperature cooling to perform H_2 chemisorption measurements. This simple procedure has been shown to give a dramatic activity decrease (compare reaction rates after activation treatments A and B in Table 3). Therefore, the uncertainty in measurements of metallic surface area has inclined us to use a metal load basis. In our opinion this fact does not significantly affect the later discussion, because metallic dispersion seems to be comparable for both nickel and cobalt catalysts and it was not greatly affected by the different activation treatments, as shown by XRDLB measurements. The use of mean crystallite diameters obtained by XRDLB to normalize the catalytic activity data is not suitable in this case, due to the likely contamination of the metallic surface, as we show later. Hence accessible metallic area can not be estimated by this technique.

Table 3 shows the acetone consumption rates obtained at 473 K. Both (C–Ni) and (C–Co) samples showed an activity decrease due to the Ar purge treatment at 773 K after H_2 reduction at 573 K (comparison between activation treatments A and B). However, whereas the (C–Ni) catalyst lost 79% of its activity, the (C–Co) catalyst only lost 15%. But when the purging time for the (C–Co) sample was increased from 20 min to 3 h (activation treatment E), the activity loss increased from 15 to 51%. This activity loss was even more pronounced (99% for nickel and 93% for cobalt) when the temperature of reduction was increased from 573 to 773 K (activation treatment D). The thermal pretreatment of the (C–Ni) catalyst in N_2 up to 573 K did not have a significant influence on the reaction rate. However, the (C–Ni)723 sample showed very little activity compared with that of (C–Ni) sample when they were both reduced at 573 K. Both (C–Ni) and (C–Co) samples showed hydrogenation activity after Ar treatment for 12 h at 723 K (activation treatment C). This activity was remarkably high for (C–Co), being 48% of that obtained after H_2 reduction at 573 K.

(ii) Acetone hydrogenation selectivity. 2-Propanol was the main product of acetone hydrogenation. However, methyl isobutyl ketone (MIBK), isopropyl ether and a cracking fraction (mainly methane and propane) were also found. Figure 7 shows the selectivity towards the different reaction products versus the overall acetone conversion for the (C–Ni) samples subjected to different activation treatments. On the basis of thermodynamic data, the calculated equilibrium acetone conversion for the acetone hydrogenation to 2-propanol under the experimental conditions used in this work is about 43%. Selectivity differences were not found between the (C–Ni), (C–Ni)423, and (C–Ni)573 samples; therefore, only the results for the (C–Ni) sample are reported. When this catalyst was reduced in flowing H_2 at 573 K, an excellent selectivity to 2-propanol was obtained, achieving 99% at an overall

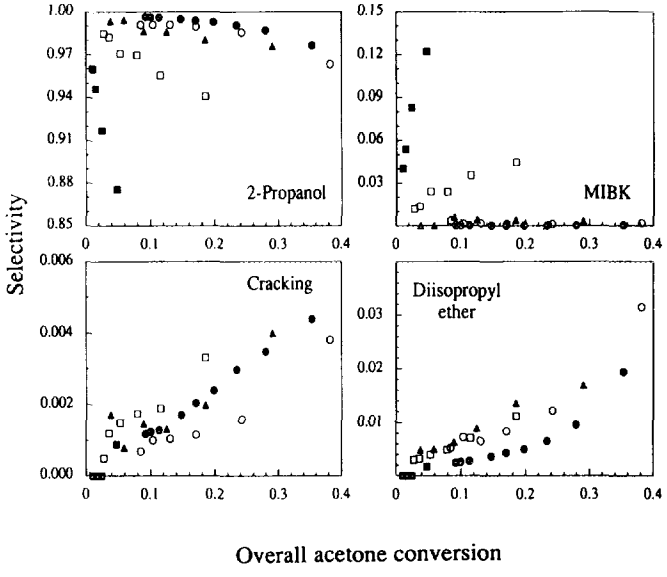

FIG. 7. 2-Propanol, methyl isobutyl ketone (MIBK), cracking products, and diisopropyl ether selectivities for the acetone hydrogenation (473 K) with the (C–Ni) sample subjected to the following activation treatments (see Table 1): A (●), B (○), C (□), D (■), and with the (C–Ni)723 sample subjected to the activation treatment A (▲).

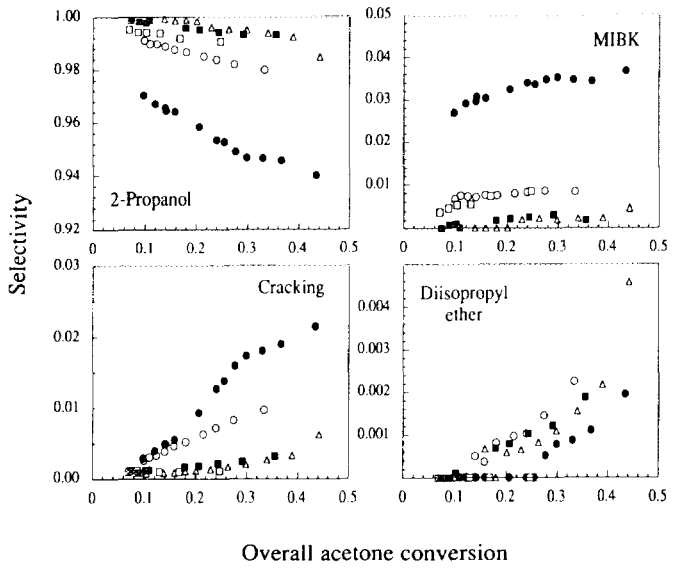

FIG. 8. 2-Propanol, methyl isobutyl ketone (MIBK), cracking products, and diisopropyl ether selectivities for the acetone hydrogenation (473 K) with the (C–Co) sample subjected to the following activation treatments (see Table 1): A (●), B (○), C (△), D (□), and E (■).

acetone conversion of 25% (Fig. 7, activation treatment A). A decrease of the 2-propanol selectivity is shown in the following order of activation treatments. When Ar purge at 773 K was performed after reduction at 573 K, a slight selectivity decrease took place that was mainly due to an increase in the formation of isopropyl ether (Fig. 7, activation treatment B). A more pronounced decrease in 2-propanol selectivity was obtained when the (C–Ni) catalyst was treated in Ar for 12 h at 723 K. In this case the formation of MIBK was favoured and a selectivity of 5% to this product was obtained at 20% overall acetone conversion (Fig. 7, activation treatment C). The lowest selectivity to 2-propanol with the (C-Ni) catalyst was achieved after H_2 reduction at 773 K. In this case 12% of MIBK selectivity was shown at 5% overall acetone conversion (Fig. 7, activation treatment D). Very low selectivities to cracking products were obtained with the (C–Ni) samples, and the activation treatment was found to have little effect. Figure 8 shows the selectivity towards the different reaction products versus the overall acetone conversion for the (C–Co) samples subjected to different activation treatments. The selectivity to 2-propanol of sample (C–Co) behaved in the opposite way to the activation treatments than that of the (C–Ni) sample. With cobalt, the lowest 2-propanol selectivity was obtained after H_2 reduction at 573 K, due to the high MIBK and cracking products selectivities obtained (Fig. 8, activation treatment A), which reached 3.5 and 1.8%, respectively, at 30% overall acetone conversion. A trend of increasing 2-propanol selectivity could be seen in the following order. Ar purge for 20 min at 773 K after reduction at 573 K produced an increase in the 2-propanol selectivity from 95 to 98% at 30% overall acetone conversion, accompanied by a decrease in the formation of MIBK (Fig. 8, activation treatment B). When the purging time was increased to 3 h an additional gain to 99% 2-propanol selectivity was obtained at the same overall conversion, due to a greater reduction in the production of cracking products (Fig. 8, activation treatment E). This increased purging time produced comparable selectivities to that of the H_2 reduction at 773 K (Fig. 8 activation treatment D) and that of the Ar treatment for 12 h at 723 K (Fig. 8, activation treatment C). This last pretreatment produced the most selective catalyst for 2-propanol found in this work, with values higher than 99.5% for overall acetone conversions lower than 30%. With the cobalt activated-charcoal-supported catalysts, selectivities to isopropyl ether lower than 0.3% were obtained for all the different activation treatments.

(iii) Metallic powders and sulfurized catalysts activity and selectivity. Samples of passivated Ni and Co powders were H_2 reduced (activation treatment D), then acetone hydrogenation was carried out at 473 K with W/F_{A0} values of 3.1 (g Ni mol acetone^{-1} h^{-1}) for nickel powder and 4.1 (g Co mol acetone^{-1} h^{-1}) for cobalt powder. Nickel showed a large conversion decay from 2.6 to 0.2% after 2 h on stream. In addition, the selectivity to 2-propanol increased from 99.5 to 100%, methane and propane being the only byproducts found. Cobalt showed a lower activity decay than nickel, with an acetone conversion decrease from 2.6 to 1.5% after 2 h of on stream. In contrast with nickel, cobalt showed very high selectivities towards acetone aldol condensation products, namely, MIBK (25 to 5%) and mesityl oxide (MSO) (17 to 3%). No cracking products were found with unsupported cobalt.

Partially sulfurized (C–Ni) catalyst showed a stable 2.5% acetone conversion (0.09 mol acetone h^{-1} g Ni^{-1}). Remarkably high selectivities to MIBK, between 21 and 9%, were obtained with this catalyst during the 2-hour experiment. Selectivities to cracking products and diisopropyl ether of around 2 and 0.8%, respectively, were also obtained. Partially sulfurized (C-Co) catalyst also showed a very stable acetone conversion of 2.6% (0.06 mol acetone h^{-1} gCo^{-1}) and MIBK selectivity between 21 and 10% during 2 h on stream. This catalyst gave a very stable selectivity (1.3%) to cracking products.

DISCUSSION

Evolution of Catalyst Texture and Structure

Thermal pretreatments up to 723 K under N_2 flow did not produce significant changes in the activated-charcoal support, as can be seen in Table 2. Therefore the surface area and porosity decrease in samples with nickel or co-

balt after different treatments must be related to the presence of different nickel or cobalt compounds. The pore blockage can be caused by nickel or cobalt nitrate, produced during the drying treatment. This pore blockage is especially favoured by the slow drying procedure used, which allows the capillary diffusion of the impregnating solution through the narrower pores (31, 32).

(C–Ni) treated at 423 K under N_2 did not show any textural parameter recovery, in agreement with TGA and XRD experiments that did not indicate nitrate decomposition.

At 573 K under N_2, both Ni and Co nitrates decompose, as can be seen from the TGA results and from the XRD patterns which show the presence of NiO and CoO. This decomposition, which is a complex process in the case of Ni, is accompanied by a volume reduction that could explain the surface area and porosity recovery.

The pretreatment at 723 K under N_2 of both parent catalysts produced an additional surface area and porosity recovery that can be related to the reduction of both oxides to the metallic form showed by the XRD patterns. This reduction process could be detected identically in both N_2 and H_2 TGA experiments (Figs. 1b and 2b for Ni and Figs. 1d and 2d for Co), and no additional reduction was produced by H_2 treatment over the previously inert gas pretreated (C–Ni)723 sample (Fig. 2c). Therefore, it can be concluded that the reduction was produced by the activated-charcoal support. These results are in agreement with those of Silva *et al.* (13).

Oh *et al.* have studied the Co/graphite system by means of in situ TEM and electron diffraction under controlled atmosphere (14). These authors have found that above 1153 K very active metallic Co particles catalyze the combustion of graphite, while nickel is much less active under the same conditions (16). As was pointed out by Oh *et al.*, the higher activity of cobalt is due to its ability to perform redox cycles at all temperatures, allowing the oxygen transfer from the gaseous atmosphere to the graphite. These authors have also pointed out that the lower activity of nickel was due to the stability of NiO, which is not reduced by the graphite. Amariglio *et al.* have also studied the combustion of graphite catalyzed by numerous elements including nickel (17). From their results, these authors concluded that the metal acts as an active oxygen carrier to the support. If we apply these mechanism to our results, we have, in contrast with Oh *et al.*, an inert atmosphere (N_2) and the metallic particles are supported on activated charcoal and not on the poorly reactive graphite. Using our experimental conditions it is not possible to take oxygen from the gaseous environment. The lower temperature required in our work, and in that of Silva *et al.* (13), to reduce nickel and cobalt oxides can be explained by the higher reducing activity of activated charcoal compared to that of graphite (1). Hence, when the (C–Ni) and (C–Co) catalysts are treated in N_2 at a sufficiently high temperature, the oxides resulting from the nitrate decomposition transfer their oxygen atoms to the support, which in turn is oxidized. The mechanism seems to be very similar to that of the transition metal catalyzed oxidation of graphite.

Attempts were made to evaluate the extent of reduction of the precursor to the metallic state due to the action of carbon. Unfortunately, analysis of the exit gases resulting from the TGA experiments is not available in our laboratories. Hence, only lower and higher limits for the extent of reduction have been calculated assuming that the TGA weight losses recorded under N_2 were due only to CO or CO_2 evolution, respectively. These limits are 79 to 100% for the (C–Ni) catalyst and 71 to 90% for the (C–Co) catalyst. The high extent of reduction obtained for the (C–Ni) catalyst is in good agreement with the XRD pattern of the (C–Ni)723 sample (Fig. 4), in which NiO is hardly detected. Nevertheless, the XRD pattern of the (C–Co)723 sample (Fig. 5) clearly shows the Co_3O_4 phase. This cobalt oxide is believed to have been formed when the (C–Co)723 sample is exposed to atmospheric oxygen after N_2 thermal treatment, which readily oxidizes the metallic cobalt previously formed to Co_3O_4. Quantitative TGA results must be analyzed carefully since the oxygen from the nickel and cobalt oxide particles does not necessarily have to be evolved as CO and/or CO_2. The oxygen can also remain in the support as surface oxygen functionalized groups (carboxylic, quinonic, phenolic, . . .) (2, 11). Hence, the observed weight loss could correspond to a complex series of processes.

It is important to compare information about the metal surface area after different activation treatments that can be deduced from H_2 chemisorption, catalytic activity, XRDLB, and TEM. H_2 chemisorption and catalytic activity data obtained showed dramatic losses after activation treatments at the higher temperatures, suggesting the importance of metal sintering. Nevertheless, XRDLB and TEM measurements showed that the metal particle size remained almost constant. The most likely explanation for these discrepancies is that some contamination of the metal surface has been produced during the activation treatment at high temperature, decreasing the chemisorbed H_2 uptake and catalytic activity of the samples.

Effect of Thermal Treatments on the Catalyst Activity

The most important observed effects of the thermal treatments are as follows:

—When the (C–Ni) catalyst was pretreated in an inert atmosphere at temperatures up to 573 K and subsequently subjected to the B activation treatment (see Table 1), both metallic surface area and catalytic activity remained almost constant. But when the inert gas pretreatment was

made at 723 K, a significant decrease of both parameters took place.

—The different activation procedures used with the two parent catalysts showed that increasing the reduction temperature or the inert purging time after reduction gave a loss in catalytic activity.

—Treatment in H_2 at 773 K resulted in noticeably higher activity loss with respect to activation treatment A than inert gas treatment at 723 K. This difference is remarkable for cobalt, taking into account the proximity of the two temperatures.

—For a given activation treatment at the higher temperatures, the activity loss is always higher for nickel than cobalt.

The important differences in catalytic activity observed can not be explained by metal sintering that could be deduced from the hydrogen chemisorption data obtained with the technique available in our laboratory. This technique needs a high-temperature purging treatment with inert gas before hydrogen chemisorption, but this treatment has been shown to produce significant activity changes. Therefore, crystallite sizes measured by XRDLB should be used for the sintering assessment. Values in Table 3 show relatively small differences between the minimum (9.1 nm) and the maximum (17.3 nm) crystallite size that can not explain the observed catalytic activity differences, covering two orders of magnitude.

A very likely explanation for this behaviour is that the support is acting as a poisoning agent. This action could be accomplished by the carbon itself and/or additionally by mineral impurities present in the support. In our case poisoning could be carried out by the sulfur found in the Norit ROX 0.8 activated charcoal, this reaching up to 0.7 wt%. This amount is high enough to seriously deactivate the catalyst if the sulfur moves to the metal surface. The different behaviour of nickel and cobalt found in this work makes it difficult to ascribe the activity loss with increasing treatments temperature to only one common deactivating agent. Therefore, the interaction of both metals with carbon and sulfur will be discussed separately.

The work of Blakely *et al.* showed that nickel (33) and cobalt (34) can be saturated with atomic carbon to its solubility limit at high temperature. When these metals are cooled, the carbon solubility rapidly decreases, and a part of the previously dissolved carbon precipitates onto the surface. The bulk to surface precipitation of carbon on polycrystalline nickel with bulk carbon concentration of the order of 0.01 at% has been studied by Mojica and Levenson (35). According to these authors, the time dependence of the process shows two steps. The first step involves carbon atoms migrating from the layers near the surface and replacing nickel atoms at the surface. The duration of this step is about 25 min at 618 K and about 10 min at 698 K. The second step involves the formation of graphitic fragments on the metal surface. These processes are very similar to those that take place at the nickel surface when the carbon deposition comes from a gaseous reactant (36). In this case, during the first stage, an α state is detected consisting of isolated surface carbon atoms bonded to the high coordination metal sites. Then, as the carbon surface coverage increases, the α state is transformed in the β state, which consists of amorphous carbon. This β state is low density carbon which is unstable with respect to the more dense and unreactive forms that deactivate the metal surface. Dumesic et al. carburized the surface of a Ni polycrystalline foil. According to these authors, carbon atoms may diffuse into the bulk above 600 K and the carbidic carbon is transformed to graphitic carbon above 700 K (20). It should be emphasized that evidence has been found in this work by TGA, XRD, and activity measurements after activation treatment C (see Table 1) that the support seems able to reduce Ni and Co precursors to the metallic state under an inert gas atmosphere. So, it is possible that when the (C–Ni) and (C–Co) catalysts are subjected to temperatures above 700 K for relatively long times, the supported NiO and CoO particles can be reduced by diffusing carbon atoms in a similar way as previously reported during the growth of filamentary carbon on a nickel catalyst (37). It seems likely that after the reduction process the metallic particles became saturated in carbon atoms. When the temperature is lowered (i.e., to ambient temperature to perform H_2 chemisorption or to 473 K for acetone hydrogenation measurements), the carbon solubility decreases and the excess of carbon can precipitate onto the metal surface evolving to more inert forms which would then be in part responsible for the activity loss.

Sulfur poisoning of transition metals due to the formation of very stable surface sulfides is a well known phenomenon. However, most of the experimental work has been concerned about sulfur coming from the gaseous phase (23). For example, Bartholomew *et al.* found that when H_2S is the poison, alumina-supported nickel and cobalt showed similar sulfur tolerance (38). In our case, sulfur is present as an impurity in the support and it has to diffuse across the carbon surface towards the metallic particles. This process will be favoured by increasing operating periods and temperatures. Once the sulfur reaches the metallic particle the formation of deactivating surface sulfides is favoured by their higher thermodynamic stability with respect to sulfur in the particle bulk (23).

In the light of the above discussion and the present experimental data, not only carbon and sulfur but also the surrounding atmosphere must play an important role, making the interpretation of the effects of thermal treatments on catalytic activity difficult. Thus, when thermal treatments are performed under an inert atmosphere, the

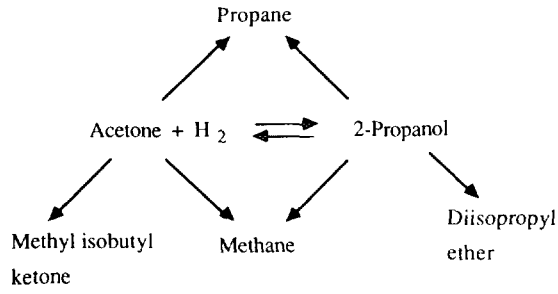

FIG. 9. Proposed acetone hydrogenation (473 K) reaction scheme over Ni and Co activated-charcoal-supported catalysts.

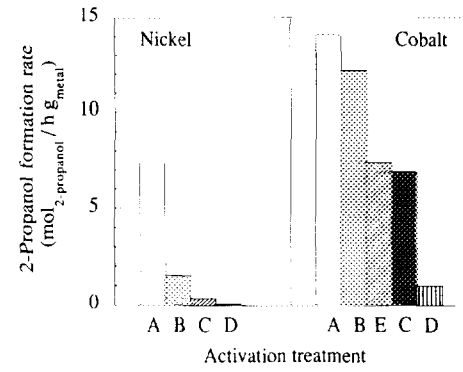

FIG. 10. 2-Propanol formation rate at 10% overall acetone conversion level with the (C–Ni) and (C–Co) samples subjected to different activation treatments (see Table 1).

conditions can be favourable to achieve high carbon oversaturations in the metal particles because the precursors are reduced by carbon. In addition, the carbon saturation of the metallic particles can hinder the sulfur action (39). Hence, these conditions seem favourable to an important contribution of carbon to the activity loss. On the other hand, the opposite situation is more likely when activation treatments are performed under H_2. In these cases, conditions can be easier for sulfur poisoning, and the high toxicity of surface sulfides could be an explanation for the more intense activity loss shown when H_2 is used in the activation treatments.

It is interesting to note that the activity losses found with thermal treatments are more important for nickel samples than for cobalt, in spite of the apparently comparable affinity and toxicity of sulfur for both metals (23, 38). However, the solubility of carbon in cobalt is considerably lower than in nickel (ca. 10 times lower at 773 K) (33, 34).

Changes in Acetone Hydrogenation Selectivity

The reported changes in acetone hydrogenation selectivity as a function of the several high temperature pretreatments could be a consequence of the very important modifications that take place in the metallic surfaces of the (C–Ni) and (C–Co) catalysts. The experimental conditions for the acetone hydrogenation employed in this work, 473 K, and a wide range of overall acetone conversions are unusual. The majority of the previously reported work on this reaction has been carried out at temperatures lower than 373 K and at very low acetone conversions. Hence, although a great variety of catalysts have been studied, the 2-propanol selectivity has been reported to be significantly affected only by small amounts of propane coming from the hydrogenolysis of the acetone carbon–oxygen double bond (40, and references therein).

Taking into account the reaction compounds identified from our experimental conditions and the related literature detailed later, the most likely overall reaction scheme is that proposed in Fig. 9. Briefly, it involves direct hydrogenation of acetone to 2-propanol. The dehydration of two 2-propanol molecules gives rise to diisopropyl ether formation. This result is in agreement with the work of Pines and co-workers (41 and references therein). These authors have studied the conversion of alcohols over nickel catalysts under experimental conditions similar to those of this work showing that dehydration to the respective ether proceeds via a concerted *trans*-elimination mechanism over an acid–base pair site. Direct formation of propane from acetone has been well established (40). This product can also originate from dehydration of 2-propanol and hydrogenation of a propene-type intermediate. The formation of methane by interaction of acetone with silica-supported nickel and cobalt at 473 K has been reported (42). Methyl isobutyl ketone (MIBK) is produced via aldol condensation of acetone. This reaction can be performed at 1 atm through acetone aldolization to diacetone alcohol (DAA), dehydration of DAA to mesityl oxide (MSO), and hydrogenation of MSO to MIBK in a single stage (43, 44).

The different activation treatments produced changes in both activity and selectivity of the catalysts. Therefore, in order to consider both characteristics, Figs. 10 to 13

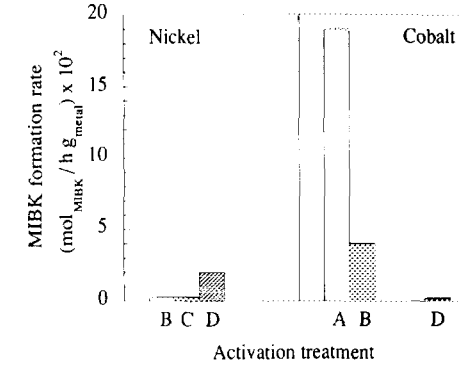

FIG. 11. Methyl isobutyl ketone (MIBK) formation rate at 10% overall acetone conversion level with the (C–Ni) and (C–Co) samples subjected to different activation treatments (see Table 1).

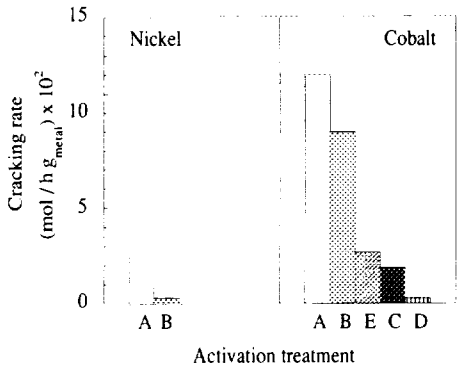

FIG. 12. Cracking products formation rate at 10% overall acetone conversion level with the (C–Ni) and (C–Co) samples subjected to different activation treatments (see Table 1).

show the formation rate of the different products (mol of product formed per h per g of metal loaded in the reactor) at 10% overall acetone conversion, as a function of the activation treatment. As a first general conclusion, it should be pointed out that the (C–Co) catalyst was more active than (C–Ni) towards the formation of 2-propanol and cracking products when these catalysts were subjected to the same activation treatments. However, isopropyl ether was only produced in significant amounts with nickel, but at a very low rate. It is also noteworthy that with both metals, the rate of formation of 2-propanol (Fig. 10) was between one and two orders of magnitude higher than that of any other product for all the activation treatments used. This led to very high selectivities to 2-propanol which, at 5% overall acetone conversion for the (C–Ni) catalyst, range between 87.5 and 99.6% depending on the activation treatment. At the same conditions, values between 97 and 99.9% were obtained for the (C–Co) catalyst.

The catalytic activity loss for nickel and cobalt produced by increasing thermal treatment time and temperature was accompanied with opposite tendencies in selectivity. These results are likely to be related to the metallic surface poisoning discussed in the previous section. The (C–Ni) catalyst showed a 2-propanol selectivity decrease with increasing activation treatments time and temperature. This behaviour was mainly due to the development of low activity for MIBK formation which, in conjunction with the very important loss of 2-propanol formation activity (see Figs. 10 and 11) caused a noticeable decrease in 2-propanol selectivity. At this point, it is interesting to note the results obtained in the experiments carried out with the metallic powders and partially sulfurized catalysts. Metallic Ni powder was not active for MIBK formation nor was the (C–Ni) catalyst subjected to activation treatments A and B. However, the sulfurized (C–Ni) catalyst showed a measurable selectivity to MIBK, as did the (C–Ni) catalyst after activation treatments C and D. Therefore, the formation of surface nickel sulfide could explain the activity and selectivity changes for the (C–Ni) catalyst with thermal treatments. The (C–Co) catalyst showed a very important increase in selectivity to 2-propanol with increasing activation treatment times and temperatures. This behaviour is due to a more resistant activity to 2-propanol formation (see Fig. 10) in conjunction with a dramatic decrease in the MIBK formation activity (see Fig. 11). Metallic cobalt powder, as well as a sulfurized (C–Co) catalyst, showed a similar and relatively high activity to MIBK. Hence the formation of surface cobalt sulfide does not agree with the selectivity pattern of the (C–Co) samples. It is difficult to explain this result, but selective blocking of active sites for MIBK formation by carbon species could be a possibility. The process of segregation of atomic carbon to the nickel or cobalt surface is highly structure sensitive (33, 34), and thus certain sites could be more affected than others.

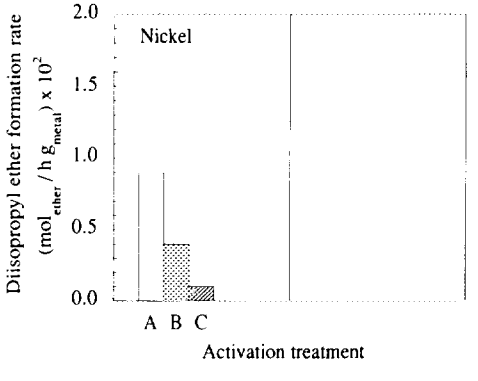

FIG. 13. Diisopropyl ether formation rate at 10% overall acetone conversion level with the (C–Ni) sample subjected to different activation treatments (see Table 1).

CONCLUSIONS

—The impregnation process with Ni and Co nitrates causes microporous surface area and volume losses in the activated-charcoal support that are partially restored during the thermal pretreatments.

—The activated-charcoal support used in this work was able to reduce both NiO and CoO to the metal when samples were treated in an inert stream above 723 K. This process can be explained by dissolution of carbon atoms in the oxide particles. N_2 or Ar thermal treatments and H_2 activation treatments above 723 K caused a great loss of acetone hydrogenation activity which was not due to metal sintering, as shown by XRD measurements. These results can be explained by two phenomena which are not mutually exclusive; the formation of surface sulfides due to the presence of sulfur as impurity in the support,

and carbon surface species produced by precipitation of bulk-dissolved carbon.

—The different inert gas and H_2 activation treatments used in this work gave rise to very important changes in the acetone hydrogenation selectivity. When both (C–Ni) and (C–Co) catalysts were subjected to a mild hydrogen reduction at 573 K, their selectivity patterns were similar to those of the respective metallic powders. The decrease of 2-propanol selectivity of the (C–Ni) catalyst subjected to more severe activation treatments is likely to be due to the formation of surface nickel sulfides. The increase of 2-propanol selectivity of the (C–Co) catalyst could be better understood by selective blocking by carbon species of the active centers in those parts of the surface responsible for MIBK formation.

—Activated charcoal has been found to be a very reactive support towards dispersed nickel and cobalt particles. During the catalyst preparation and activation treatments, several processes can occur, such as metallic precursor reduction by the support and metal surface contamination. Therefore, physicochemical characterization data should be analysed and checked carefully.

—It is interesting to note the remarkably high selectivities to 2-propanol found in this work under severe and unusual experimental conditions (473 K). Selectivities higher than 99% for (C–Ni) H_2 reduced at 573 K and 99.6% for (C–Co) Ar treated at 723 K were found. This fact makes these two catalysts very promising candidates to selectively hydrogenate acetone in a high-temperature chemical heat pump application.

ACKNOWLEDGMENTS

We express our thanks to A. Gil for nitrogen adsorption measurements, to A. Díaz for TEM observations, and to Dr. P. D. Armitage for reviewing the manuscript. The scholarship support for L. M. Gandía by the Ministerio de Educación y Ciencia (Programme FPI) and the financial support by the Gobierno Vasco (Grant GV 89 Nº A9) are gratefully appreciated.

REFERENCES

1. Cameron, D. S., Cooper, S. J., Dogson, I. L., Harrison, B., and Jenkins, J. W., *Catal. Today* **7,** 113 (1990).
2. Albers, P., Deller, B.M., Despeyroux, B. M., Schäfer, A., and Seibold, K., *J. Catal.* **133,** 467 (1992).
3. Duchet, J. C., Van Oers, E. M., De Beer, V. H. J., and Prins, R., *J. Catal.* **80,** 386 (1983).
4. Laine, J., Severino, F., Labady, M., and Gallardo, J., *J. Catal.* **138,** 145 (1992).
5. Lee, J. S., Oyama, S. T., and Boudart, M., *J. Catal.* **106,** 125 (1987).
6. Oyama, S. T., *Catal. Today* **15,** 179 (1992).
7. Bett, J. A., Kinoshita, K., Stonehart, P., *J. Catal.* **35,** 307 (1974).
8. Ehrburger, P., Mahajan, O. P., and Walker, P. L., Jr., *J. Catal.* **43,** 61 (1976).
9. Prado-Burguete, C., Linares-Solano, A., Rodríguez-Reinoso, F., and Salinas-Martínez de Lecea, C., *J. Catal.* **115,** 98 (1989).
10. Prado-Burguete, C., Linares-Solano, A., Rodríguez-Reinoso, F., and Salinas-Martínez de Lecea, C., *J. Catal.* **128,** 397 (1991).
11. Puri, B. R., *in* "Chemistry and Physics of Carbon" (P. L. Walker, Jr., Ed.), Vol. 6, p. 191. Dekker, New York, 1970.
12. Oades, R. D., Morris, S. R., and Moyes, R. B., *Catal. Today* **7,** 199 (1990).
13. Silva, I. F., Fernandes, F. M. B., and Lobo, L. S., *in* "Actas del XIII Simposio Iberoamericano de Catálisis, Segovia, 1992," Vol 2, p. 841.
14. Oh, S. G., and Baker, R. T. K., *J. Catal.* **128,** 137 (1991).
15. Tomita, A., and Tamai, Y., *J. Catal.* **27,** 293 (1972).
16. Baker, R. T. K., and Sherwood, R. D., *J. Catal.* **70,** 198 (1981).
17. Amariglio, H., and Duval, X., *Carbon* **4,** 323 (1966).
18. Keep, C. W., Terry, S., and Wells, M., *J. Catal.* **66,** 451 (1980).
19. Tomita, A., and Tamai, Y., *J. Phys. Chem.* **78,** 2254 (1974).
20. Raupp, G. B., and Dumesic, J. A., *J. Catal.* **95,** 587 (1985).
21. Bartholomew, C. H., *in* "Hydrogen Effects in Catalysis" (Z.Páal and D. G. Menon, Eds.), p. 146. Dekker, New York, 1988.
22. Rodríguez-Reinoso, F., Rodríguez-Ramos, I., Moreno-Castilla, C., Guerrero-Ruíz, A., and López-González, J. D., *J. Catal.* **99,** 171 (1986).
23. Bartholomew, C. H., Agrawal, P. K., and Katzer, J. R., *Adv. Catal.* **31,** 135 (1982).
24. Gandía, L. M., and Montes, M., *Int. J. Energy Res.* **16,** 851 (1992).
25. Marczenko, Z., "Separation and Spectrophotometric Determination of Elements." Ellis Horwood, Chichester, 1976.
26. Klug, H. P., and Alexander, L. E., "X-Ray Diffraction Procedures," p. 618. Wiley, New York, 1974.
27. Coenen, J. W. E., and Linsen, B. G., *in* "Physical and Chemical Aspects of Adsorbents and Catalysts" (B. G. Linsen, Ed.), p. 471. Academic Press, New York, 1970.
28. Reuel, R. C., and Bartholomew, C. H., *J. Catal.* **85,** 63 (1984).
29. Gil, A., Díaz, A., and Montes, M., *J. Chem. Soc. Faraday Trans.* **87,** 791 (1991).
30. Planinsek, F., and Newkirk, J. B., *in* "Kirk–Othmer Encyclopedia of Chemical Technology," Vol. 6, p. 481. Wiley, New York, 1979.
31. Mile, B., Stirling, D., Zammitt, M., Lovell, A., and Webb, M., *J. Catal.* **114,** 217 (1988).
32. Mile, B., Stirling, D., Zammitt, M., Lovell, A., and Webb, M., *J. Mol. Catal.* **62,** 179 (1990).
33. Isett, L. C., and Blakely, J. M., *Surf. Sci.* **58,** 397 (1976).
34. Hamilton, J. C., and Blakely, J. M., *Surf. Sci.* **91,** 199 (1980).
35. Mojica, J. F., and Levenson, L. L., *Surf. Sci.* **59,** 447 (1976).
36. McCarty, J. G., and Wise, H., *J. Catal.* **57,** 406 (1979).
37. Baker, R. T. K., Barber, M. A., Harris, P. S., Feates, F. S., and Waite, R. J., *J. Catal.* **26,** 51 (1972).
38. Bartholomew, C. H., Weatherbee, G. D., and Jarvi, G. A., *J. Catal.* **60,** 257 (1979).
39. Wise, H., McCarty, J., and Oudar, J., *in* "Deactivation and Poisoning of Catalysts" (J. Oudar and H. Wise, Eds.), p. 15. Dekker, New York, 1985.
40. Sen, B., and Vannice, M. A., *J. Catal.* 113, 52 (1988).
41. Kraus, L. S., Pines, H., and Butt, J. B., *J. Catal.* **128,** 337 (1991).
42. Blyholder, G., and Shihabi, D., *J. Catal.* **46,** 91 (1977).
43. Papa, A. J., and Sherman, P. D., Jr., *in* "Kirk–Othmer Encyclopedia of Chemical Technology," Vol. 13, p. 907, Wiley, New York, 1979.
44. Gandía, L.M., and Montes, M., *Appl. Catal. A: General* **101,** L1 (1993).